This is the peer-reviewed, final accepted version for American Mineralogist, published by the Mineralogical Society of America.
The published version is subject to change. Cite as Authors (Year) Title. American Mineralogist, in press.
DOI: https://doi.org/10.2138/am-2021-7827. http://www.minsocam.org/

Experimental Determination of Solubility Constants of Saponite at Elevated Temperatures in High Ionic Strength Solutions, Revision 1

Yongliang Xiong[1]

Department of Nuclear Waste Disposal Research & Analysis,
Sandia National Laboratories (SNL), 1515 Eubank Boulevard SE, Albuquerque, NM 87123, USA

[1] Corresponding author, e-mail: yxiong@sandia.gov.

This is the peer-reviewed, final accepted version for American Mineralogist, published by the Mineralogical Society of America.
The published version is subject to change. Cite as Authors (Year) Title. American Mineralogist, in press.
DOI: https://doi.org/10.2138/am-2021-7827. http://www.minsocam.org/

ABSTRACT

Saponite occurs in a wide range of environments from hydrothermal systems on the Earth to surface deposits on Mars. Of practical importance is that Mg-saponite forms when glasses for nuclear waste are altered in Mg-bearing aqueous solutions. In addition, saponite is favorably considered as candidate buffer materials for the disposal of high-level nuclear waste and spent nuclear fuel in harsh environments. However, the thermodynamic properties, especially for Mg-saponites, are not well known. Here the author synthesized Mg-saponite (with nitrate cancrinite) following a previously reported procedure and performed solubility experiments at 80 ºC to quantify the thermodynamic stability of this tri-octahedral smectite in the presence of nitrate cancrinite. Then, in combination with the equilibrium constant at 80 ºC for the dissolution reaction of nitrate cancrinite from the literature, the author determined the solubility constant of saponite at 80 ºC based on the solution chemistry for the equilibrium between saponite and nitrate cancrinite, approaching equilibrium from the direction of supersaturation, with an equilibrium constant of –69.24 ± 2.08 (2σ) for dissolution of saponite at 80 ºC. Furthermore, the author extrapolated the equilibrium constant at 80 ºC to other temperatures (i.e., 50 ºC, 60 ºC, 70 ºC, 90 ºC and 100 ºC) using the one-term isocoulombic method. These equilibrium constants are expected to find applications in numerous fields. For instance, according to the extrapolated solubility constant of saponite at 50 ºC and 90 ºC, the author calculated the saturation indexes with regard to saponite for the solution chemistry from glass corrosion experiments at 50 ºC and 90 ºC from the literature. The results are in close agreement with the experimental

observations. This example demonstrates that the equilibrium constants determined in this study can be used for reliable modeling of the solution chemistry of glass corrosion experiments.

INTRODUCTION

Saponite, a tri-octahedral smectite, occurs in a wide range of environments. For instance, it occurs in igneous rocks as hydrothermal alteration products (e.g., Kohyama et al., 1973; April and Keller, 1992; Garvie and Metcalf, 1997), and in metamorphosed dolomitic limestone as hydrothermal products (e.g., Post, 1984). It also occurs as lake sediments and in volcanic rocks on seafloor (e.g., Desprairies et al., 1989; Cuevas et al., 2003; Kadir and Akbulut, 2003). Its occurrence in the Martian meteorites and its proposed occurrence in Mawrth Vallis region and Yellowknife Bay, Gale Crater on Mars (e.g., Bishop et al., 2013; Hicks et al., 2014; Bristow et al., 2015) generated enormous scientific interest. Most recently, saponite was also observed in an analog study of the hydrothermal alteration in the martian subsurface (e.g., Sueoka et al., 2019; Calvin et al., 2020).

Additionally, of practical importance and therefore particular interest is that saponite is relevant to the geological disposal of nuclear waste, as Mg-saponite has been observed as an alteration product when a borosilicate glass for nuclear waste is corroded (Thien et al., 2010) in Mg-containing solutions, as detailed below.

Mg-bearing groundwaters are common in the disposal concepts in various rock formations. For instance, salt formations have been recommended for nuclear waste isolation since the 1950's by the U.S. National Academy of Science (1957). Because of their excellent properties of high heat conduction, low permeability and a propensity to self-seal, rock salt is a viable candidate for a nuclear waste repository. Salt formations contain brines, which have relatively high concentrations of magnesium (Nishri et al.,

1988; Schussler et al., 2001; Xiong and Lord, 2008). For instance, the Q-brine at Asse, Germany, has a magnesium concentration of 4.47 $mol \cdot kg^{-1}$ (Nishri et al., 1988; Schussler et al., 2001). When high level waste (HLW) glass is corroded in Mg-rich brines, Mg-bearing phyllosilicates form as part of the secondary phase assemblage (Strachan, 1983; Strachan et al., 1984; Grambow and Muller, 1989; Maeda et al., 2011). Although previously, and tentatively, identified as sepiolite (a member of the palygorskite family), more recent investigations have identified trioctahedral smectites, such as saponite with various stoichiometries, e.g., $(½Ca,Na)_{0.66}Mg_6[(Si_{7.34}Al_{0.66})O_{20}](OH)_4$(e.g., Abdelouas et al., 1997; Thien et al., 2010; Zhang et al., 2012; Fleury et al., 2013; Debure et al., 2016; Aréna et al., 2017) as a reaction product. Note that in these more recent investigations, the concentration of Mg in solution is relatively low (milli-molal range), in accord with the dilute nature of pore water chemical compositions recovered from silicate-dominated prospective repositories (e.g., Gaucher et al., 2009). Other investigations have shown that when Mg-bearing glass, such as the British Magnox compositions, is altered in dilute aqueous solutions the released Mg also leads to formation of Mg-smectite phases (e.g., Curti et al., 2006; Thien et al., 2012; Harrison, 2014). It is likely, therefore, that saponite could be a thermodynamically stable phase that precipitates when Mg-bearing solutions, both dilute and concentrated, contact silicate glass for a sufficient length of time.

When saponite forms, it may impact the near-field chemistry of a geological repository in various rock formations including salt formations by: (1) Controlling the chemical compositions, including hydrogen ion concentrations, of the contacting solutions, and (2) Forming a secondary mineral assemblage that will either enhance for certain periods (Lucksheiter and Nesovic, 1998; Curti et al., 2006; Fleury et al., 2013;

Aréna et al., 2016, 2017), or retard (Grambow and Strachan, 1984; Frugier et al., 2005) or both at different periods (Thien et al., 2012; Harrison, 2014), the dissolution rate of glasses, and impact the retention of hazardous (radioactive) constituents after release from the glass (e.g., Abdelouas et al., 1997).

In addition, because saponite has the swelling and sorption properties similar to those of montmorillonite, saponite has also been proposed as a candidate buffer material for HLW and spent nuclear fuel disposal in harsh environments (e.g., Yang et al., 2014). This is because tri-octahedral smectites such as saponite have higher thermal and chemical stabilities than di-octahedral smectites such as montmorillonite, and are less susceptible to alteration in harsh environments (e.g., Eberl et al., 1978; Güven, 1990).

Because the phyllosilicates that form on the glass surface are typically not well crystallized, and phase characterization efforts by X-ray diffraction are often technically challenging, some investigators have resorted to using solution modelling to infer the identity of candidate phases (c.f., Grambow and Müller, 1989). For this strategy to be viable, knowledge of the thermodynamic properties of eligible phases, such as saponite, is crucial. However, the thermodynamic properties of saponite, especially Mg-enriched saponite, are not well-defined, and few studies have attempted to obtain them via glass corrosion experiments (Aréna et al., 2017; Debure et al., 2016). For instance, in a recent study, Aréna et al. (2017) tried to calculate the solubility constant of saponite (they called it Mg-smectite) via geochemical modeling of their glass corrosion experiments. However, their experiments were not designed, nor were they ideal, for determining the solubility constants of saponite. Aluminum concentrations were very low in their experiments, hampering modelling efforts. Hence, several compensating hypotheses

were constructed to estimate aluminum concentrations, including: (1) that aluminium concentrations were equal to the quantification limit of the instrument (ICP-AES); (2) aluminum concentrations were equal to the quantification limit divided by 1000; and (3) aluminium was depleted stoichiometrically from saponite. These assumptions may not be warranted.

Without accurate knowledge of the thermodynamic properties of saponite, it is difficult to make reliable and accurate predictions for the evolution of chemical compositions of the solutions containing Mg interacting with glass. Accurate knowledge of its thermodynamic properties is thus the prerequisite for modeling glass corrosion in Mg-bearing solutions, both at high and low ionic strength.

The objective of this study is to determine experimentally the solubility constants of hydrous saponite at elevated temperatures under well constrained conditions. The author first synthesized saponite (from nitrate cancrinite) according to an established methodology (see Experimental Methods). Because hydrogen ion concentrations are a key parameter governing the dissolution of saponite, the author first measured pH and then applied correction factors obtained at elevated temperatures (Kirkes and Xiong, 2018). With proper knowledge of the hydrogen ion concentrations and the concentrations of Al, Mg, Na and Si in solution, the author calculated the equilibrium quotients. Then, the appropriate activity coefficient model is applied to extrapolate equilibrium quotients at certain ionic strengths to infinite dilution. This model allows us to then assess the solubility of saponite in previously reported experiments. It is shown that an accurate log K value can be used to understand glass corrosion in Mg-bearing solutions under a variety of geochemical conditions.

130

131 **EXPERIMENTAL METHODS**

132 In this study, the chemicals used for synthesis of the starting material were ACS
133 reagent grade chemicals. The synthesis followed the procedure of Shao and Pinnavai
134 (2010) with some modifications. In the work of Shao and Pinnavai (2010), the sources
135 for Al, Mg, Na and Si, were $Al(NO_3)_3 \bullet 9H_2O$, $Mg(NO_3)_2 \bullet 6H_2O$, and water glass solution
136 (containing 27 wt.% Si and 14 wt.% NaOH), respectively. In this work, the source for Si
137 is $Na_2SiO_3 \bullet 9H_2O$, and NaOH was used to control the pH_m conditions. Other reagents are
138 the same as those in Shao and Pinnavai (2010). Deionized water (DI) with >18.3 MΩ·cm
139 used in the experiments was purged with high purity Ar gas for a minimum of one hour
140 to remove dissolved CO_2, following the procedure of Wood et al. (2002) and Xiong
141 (2008).

142 A supersaturation experiment was conducted at 80.0 ± 0.5 °C as follows. First,
143 the author synthesized a mixture of saponite and nitrate cancrinite at 90 °C following the
144 procedure of Shao and Pinnavai (2010). The author kept the synthesized solid mixture
145 together with the mother solution in the same container in an oven at 90 °C for 7 days.
146 Then, the author transferred the container to another oven at 80 °C. Because aluminum
147 silicates such as zeolites exhibit prograde solubility (i.e., higher solubility at higher
148 temperatures) (Xiong, 2013), it is considered that the experiment initially kept at 90 °C
149 for some time, and then remained at 80 °C, approaches the equilibrium from the direction
150 of supersaturation.

151 Solution samples were periodically withdrawn from the experiments. Before each
152 sampling, pH readings were taken for each experiment. In each sampling, about 3 mL of

This is the peer-reviewed, final accepted version for American Mineralogist, published by the Mineralogical Society of America.
The published version is subject to change. Cite as Authors (Year) Title. American Mineralogist, in press.
DOI: https://doi.org/10.2138/am-2021-7827. http://www.minsocam.org/

153 solution was taken from each experiment, and the solution samples were filtered through
154 a 0.2 μm filter, and transferred into pre-weighed 10 mL Grade A volumetric flasks. After
155 filtration, masses of each solution sample were determined with a balance that is precise
156 to the fourth decimal place. Samples were then immediately acidified with 0.5 mL of the
157 Optima® Grade concentrated HNO_3 from Fisher Scientific, and diluted to 10 mL with DI
158 water. Chemical analyses for sodium, magnesium, aluminum, and silica were performed
159 using a PerkinElmer Optima 8300 Dual View (DV) ICP-AES.

160 The pH readings were measured with an Orion-Ross combination pH glass
161 electrode, coupled with an Orion Research EA 940 pH meter that was calibrated with
162 three pH buffers (pH 4, pH 7, and pH 13) at the experimental temperature of 80 ± 0.5°C.
163 The pH scale used in this work is the concentration scale (Mesmer and Holmes, 1992),
164 denoted as pH_m, which is a negative logarithm of hydrogen ion concentration on a molal
165 scale. The pH readings are converted to pH_m, according to the following equation (Xiong
166 et al., 2010),

167

168 $$pH_m = pH_{ob} + A_m = pH_{ob} + A_M - \log \Theta$$

169

170 where A_m and A_M are correction factors on a molal scale and a molar scale, respectively,
171 and Θ is a conversion factor from molality to molarity. In this study, the expression of
172 correction factors as a function of ionic strength at 80 °C determined for NaCl solutions
173 from Kirkes and Xiong (2018) is used to calculate the correction factors for the ionic
174 strengths of the experiment.

175 Solid phases were analyzed using a Bruker D8 Advance X-ray diffractometer
176 with a Sol-X detector. XRD patterns were collected using CuKα radiation at a scanning
177 rate of 0.667°/min for a 2θ range of 10–90°.

178 Major elemental compositions (Na_2O, Al_2O_3, MgO and SiO_2) of the saponite
179 crystals were determined by electron microprobe analysis (EMPA) at Sandia National
180 Laboratory, Albuquerque. Analyses were obtained using a JEOL JXA-8530F hyperprobe
181 electron probe micro analyzer with a field emission electron gun. The beam conditions
182 were <1 μm spot size, 15 keV accelerating potential and a current of 20 nanoamps.
183 Concentrations (wt.% oxide) were determined using Wavelength Dispersive
184 Spectrometry (WDS) to count on separate X-ray peaks judiciously chosen for efficiency,
185 performance and lack of interference. Background offsets were chosen at least 500 steps
186 away from the peak centers. Concentrations were quantified by comparing counts from
187 simple silicate standards whose chemical compositions are known. A table that lists the
188 element, the lower limit of detection, or LLD (wt. %), the crystal diffractometer and the
189 counting times is provided (Appendix A).

190 Concentrations of the major elements in saponite were determined by averaging
191 27 points. Adsorbed water was determined by loss on ignition (LOI) by heating a sample
192 to 700 °C for one hour using a Netzsch STA 409 thermal gravimetric analyzer (TGA).
193 The chemical formula of the saponite was calculated on the basis of $O_{20}(OH)_4$ per
194 formula unit.

195 SEM and EDS analyses were performed using a JEOL JSM-5900LV scanning
196 electron microscope (SEM) imaging system coupled with a NORAN System 7 Spectral
197 Analysis System for energy dispersive spectroscopy (EDS).

198

199 **RESULTS**

200 XRD pattern of the synthesized saponite is presented in Figure 1. As is shown,
201 this pattern is in reasonable agreement with that for saponite 15Å (PDF 00-013-0086)
202 (Figure 1). Notice that saponite 15Å is a pure end-member of magnesium saponite with a
203 chemical formula of $Mg_3(Si, Al)_4O_{10}(OH)_2 \bullet 4H_2O$. The peak at $2\theta \sim 60^o$, characteristic of
204 saponite, is present in the saponite synthesized in this work (Figure 1), which was also
205 observed in saponite synthesized at 160 °C by other researchers (i.e., He et al., 2014).
206 The d-spacings of the major peaks for the synthesized saponite compare well with those
207 of saponite 15Å standard (see Appendix B). In the synthesized saponite, there are some
208 concentrations of sodium, as indicated by EMPA (Table 1) and SEM-EDS analyses
209 (Figure 2). As my synthesis method follows that of Shao and Pinnavaia (2010), in which
210 it was known that there was nitrate cancrinite in addition to saponite, the two extra peaks
211 at $2\theta = 13.97^o$ and 27.48^o in Figure 1 can be attributed to nitrate cancrinite (Hund, 1984;
212 Liu et al., 2005).

213 Interestingly, the flower-like morphology of the synthetic saponite produced in
214 this study (see Figure 2A, 2B, 2C), is very similar to that observed for saponite
215 precipitated on the surface of vitrified intermediate level nuclear waste corroded in a
216 calcium-rich, magnesium-bearing solution (see Figure 4b in Utton et al., 2013). The
217 saponite in Utton et al. (2013) has a general formula of
218 $Ca_{0.25}(Mg,Fe)_3[(Si,Al)_4O_{10}](OH)_2 \bullet n(H_2O)$. The calcium in the saponite reported in Utton
219 et al. (2013) comes from the high Ca solutions that reacted with glass. In the corrosion
220 experiments of the nuclear waste glass in 0.016 $mol \bullet kg^{-1}$ $MgCl_2$ at 50 °C performed by

Thien et al. (2010), the morphology of the corrosion product saponite (see Figure 1 in Thien et al., 2010) is also similar to that of the synthetic saponite in this study. In Thien et al. (2010), the stoichiometry of the saponite is $Na_{0.39}(Mg_{2.25}Li_{0.06}Al_{0.06}Fe_{0.06}M_{0.25})[(Si_{3.23}Al_{0.77})O_{20}](OH)_4$, where M is a cation as Ni^{2+} or Mn^{2+}. This stoichiometry is similar to that of the saponite synthesized in this study (see below).

According to EPMA analysis, the stoichiometry of saponite synthesized in this work is $Na_{0.95}(Mg_{5.90}Al_{0.06})[(Si_{7.07}Al_{0.93})O_{20}](OH)_4$. The structural formula is calculated by normalizing cation compositions to a theoretical structure containing $O_{20}(OH)_4$. The total weight loss (loss on ignition, LOI) up to 700 ºC is 19 wt%, similar to that for the natural saponite from California (Post, 1984), which has a total weight loss of 16.66 wt% (Table 1). The stoichiometry of the natural saponite from Ballarat, California, is calculated as $(Ca,Na,K)_{0.75}(Mg_{5.17}Al_{0.31}Fe^{III}_{0.13})[(Si_{7.55}Al_{0.45})O_{20}](OH)_4$ (Table 1). The natural saponite from Milford, Utah, has a LOI of 17.30 wt% (Cahoon, 1954), and its stoichiometry is calculated as $(Ca,Na,K)_{0.42}(Mg_{5.72}Al_{0.19}Fe^{III}_{0.02})$ $[(Si_{7.50}Al_{0.50})O_{20}](OH)_4$ (Table 1). In addition, the stoichiometry of the natural saponite from Allt Ribhein, Skye, is $(Ca,Na,K)_{1.02}(Mg_{5.84}, Mn_{0.01}, Al_{0.03}, Fe^{III}_{0.08})[(Si_{6.99}Al_{1.01})O_{20}](OH)_4$ (MacKenzie, 1957) (Table 1). Therefore, the stoichiometry of natural saponite varies to some degree. The stoichiometric coefficients for Mg are similar in saponite from these localities, suggesting they belong to Mg-saponite. Notice that the stoichiometry of the synthetic saponite is similar to that from Allt Ribhein, Skye, in terms of Si, Al, and Mg.

In this study, the solubility experiment at 80 ± 0.5 ºC was performed from the direction of supersaturation to approach equilibrium (see Experimental Methods section

This is the peer-reviewed, final accepted version for American Mineralogist, published by the Mineralogical Society of America.
The published version is subject to change. Cite as Authors (Year) Title. American Mineralogist, in press.
DOI: https://doi.org/10.2138/am-2021-7827. http://www.minsocam.org/

for details). The experimental results for pH_m, sodium, total magnesium, total aluminum, total silica, nitrate and hydroxyl concentrations are presented in Table 2 and are displayed in Figure 3. It is clear from Figure 3 that steady state conditions were achieved for all solutes in terms of concentration with deviations generally ≤ 25% on a linear scale. For instance, the sodium concentrations remain between 1.38 and 1.44 mol•kg^{-1}, a deviation of 4%. Note that Al and Si usually vary reciprocally for the dissolution of Al-silicates, and it is appropriate to assess their variations using the solubility product of both Al and Si (i.e., $m_{\Sigma Al} \times m_{\Sigma Si}$) (Xiong, 2016). As nitrate cancrinite and saponite are in equilibrium in our experiment, the equilibrium constant for the assemblage of nitrate cancrinite and saponite can be determined, based on the experimental results.

The equilibrium between saponite and nitrate cancrinite in alkaline solutions can be written as follows:

$$Na_{0.95}Mg_{5.90}[(Si_{7.07}Al_{0.99})O_{20}](OH)_4 + 2NO_3^- + 7.05Na^+ + 5.01Al(OH)_4^- \rightleftharpoons Na_8[Al_6Si_6O_{24}](NO_3)_2\bullet 4H_2O + 5.90Mg^{2+} + 9.62OH^- + 1.07H_2SiO_4^{2-} + 2.14\ H_2O(l) \quad (1)$$

The equilibrium quotient for Reaction (1) is:

$$Q_1 = \frac{(m_{Mg^{2+}})^{5.90} \times (m_{H_2SiO_4^{2-}})^{1.07} \times (m_{OH^-})^{9.62}}{(m_{Na^+})^{7.05} \times (m_{NO_3^-})^2 \times (m_{Al(OH)_4^-})^{5.01}} \quad (2)$$

The equilibrium constant at infinite dilution is:

This is the peer-reviewed, final accepted version for American Mineralogist, published by the Mineralogical Society of America.
The published version is subject to change. Cite as Authors (Year) Title. American Mineralogist, in press.
DOI: https://doi.org/10.2138/am-2021-7827. http://www.minsocam.org/

$$K_1^0 = Q_1 \times \frac{(\gamma_{Mg^{2+}})^{5.90} \times (\gamma_{H_2SiO_4^{2-}})^{1.07} \times (\gamma_{OH^-})^{9.62} \times (a_{H_2O})^{2.14}}{(\gamma_{Na^+})^{7.05} \times (\gamma_{NO_3^-})^{2} \times (\gamma_{Al(OH)_4^-})^{5.01}} \quad (3)$$

In the above equations, m_i denotes a concentration for the i-th species on a molal scale, mol•g^{-1}; γ_i an activity coefficient for the i-th species; and a_{H_2O} activity for water. The equilibrium quotient for Reaction (1) at 80 °C is listed in Table 3.

Similarly, the dissolution reaction for nitrate cancrinite in alkaline solutions can be expressed as:

$$Na_8[Al_6Si_6O_{24}](NO_3)_2 \bullet 4H_2O + 12OH^- + 8H_2O(l) \rightleftharpoons 8Na^+ + 6Al(OH)_4^- + 6H_2SiO_4^{2-} + 2NO_3^- \quad (4)$$

The equilibrium quotient for Reaction (4) can be expressed as:

$$Q_4 = \frac{(m_{Na^+})^8 \times (m_{NO_3^-})^2 \times (m_{Al(OH)_4^-})^6 \times (m_{H_2SiO_4^{2-}})^6}{(m_{OH^-})^{12}} \quad (5)$$

The corresponding equilibrium constant at infinite dilution is:

$$K_4^0 = Q_4 \times \frac{(\gamma_{Na^+})^8 \times (\gamma_{NO_3^-})^2 \times (\gamma_{Al(OH)_4^-})^6 \times (\gamma_{H_2SiO_4^{2-}})^6}{(\gamma_{OH^-})^{12} \times (a_{H_2O})^8} \quad (6)$$

Bickmore et al. (2001) determined a value of $\log_{10} K^0 = -36.2 \pm 0.6$ (2σ) for Reaction (4) at 89 °C. Lichtner and Felmy (2003) provided a value of $\log_{10} K^0 = -39.03$

This is the peer-reviewed, final accepted version for American Mineralogist, published by the Mineralogical Society of America.
The published version is subject to change. Cite as Authors (Year) Title. American Mineralogist, in press.
DOI: https://doi.org/10.2138/am-2021-7827. http://www.minsocam.org/

at 75 °C. The linear interpolation of these two values leads to a value of –37.99 ± 0.70 (2σ) for Reaction (4) at 80 °C (Table 3). This value is used to retrieve the solubility constant for saponite at 80 °C as detailed below.

In our thermodynamic calculations for the activity coefficients for Equations (3) an (6), we use the computer code EQ3/6 Version 8.0a (Wolery et al., 2010; Xiong, 2011). In all calculations, the activity of all solid phases is assumed to be unity. The EQ3/6 code has been successfully used as a modeling platform in a number of previous studies at ambient temperature (e.g., Xu et al., 1999; Kong et al., 2013; Xiong, 2015, 2020) and at elevated temperatures up to 523.15 K (e.g., Xiong, 2013, 2014, 2016).

The database used for thermodynamic calculations is DATA0.YPF (Wolery and Jarek, 2003), which utilizes the Pitzer model for calculations of activity coefficients of aqueous species. The database was modified with the addition of the Pitzer parameters and equilibrium constants for Al and Si species from Xiong (2013 and 2014).

Based on the experimental data, we first calculated the equilibrium constant for Reaction (1) (Table 3). The equilibrium constant for Reaction (1) at infinite dilution and 80 °C is –31.25 ± 1.96 (2σ) in logarithmic units (Table 3).

The combination of Reactions (1) and (4) leads to,

$$Na_{0.95}Mg_{5.90}[(Si_{7.07}Al_{0.99})O_{20}](OH)_4 + 2.38OH^- + 5.86H_2O(l) \rightleftharpoons 0.95Na^+ + 5.90Mg^{2+} + 0.99Al(OH)_4^- + 7.07H_2SiO_4^{2-} \quad (7)$$

The equilibrium quotient for Reaction (7) can be expressed as:

This is the peer-reviewed, final accepted version for American Mineralogist, published by the Mineralogical Society of America.
The published version is subject to change. Cite as Authors (Year) Title. American Mineralogist, in press.
DOI: https://doi.org/10.2138/am-2021-7827. http://www.minsocam.org/

$$Q_7 = \frac{(m_{Na^+})^{0.95} \times (m_{Mg^{2+}})^{5.90} \times (m_{Al(OH)_4^-})^{0.99} \times (m_{H_2SiO_4^{2-}})^{7.07}}{(m_{OH^-})^{2.38}} \quad (8)$$

The corresponding equilibrium constant at infinite dilution is:

$$K_7^0 = Q_7 \times \frac{(\gamma_{Na^+})^{0.95} \times (\gamma_{Mg^{2+}})^{5.90} \times (\gamma_{Al(OH)_4^-})^{0.99} \times (\gamma_{H_2SiO_4^{2-}})^{7.07}}{(\gamma_{OH^-})^{2.38} \times (a_{H_2O})^{5.86}} \quad (9)$$

According to the equilibrium constants for Reactions (1) and (4), the equilibrium constant for dissolution of saponite at 80 ºC in alkaline solutions (i.e., pH_m ~12.58), represented by Reaction (7), is computed to be –69.24 ± 2.08 (2σ) in logarithmic units (Table 3). The quoted uncertainty includes the error propagations.

DISCUSSIONS

Debure et al. (2016) conducted three glass corrosion experiments with the International Simple Glass (G_{ISG}) at 90 ºC. The first one involved pure water, the second experiment used 8×10^{-3} mol•dm^{-3} $MgCl_2$ as the Mg-source, and the third corrosion experiment was conducted in the presence of hydromagnesite. In their experiments with $MgCl_2$ and hydromagnesite, it was observed that Mg-phyllosilicates (saponite) were formed as white crusts on the glass powder surface, whereas no Mg-phyllosicates were observed in the experiment with pure water. Because, for their corrosion experiment with hydromagnesite, they determined a complete set of chemical compositions for the solution, that experiment is an appropriate candidate to test the solubility constant of

saponite determined in this study. In the test, this author calculates the saturation index for saponite at 90 °C with the stoichiometry determined in this study for the experimental solution in Debure et al. (2016) at the same temperature.

In the calculations, the author first extrapolated the solubility constant of saponite determined at 80 °C to the experimental temperature of 90 °C in Debure et al. (2016). In the extrapolation, the author uses the one-term isocoulombic approach (Gu et al., 1994) for the following semi-isocoulombic reaction, utilizing ionization of water as a model substance to balance the charges for the reaction:

$$Na_{0.95}Mg_{5.90}[(Si_{7.07}Al_{0.99})O_{20}](OH)_4 + 15.13OH^- + 12.75H^+ \rightleftharpoons 0.95Na^+ + 5.90Mg^{2+} + 0.99Al(OH)_4^- + 7.07H_2SiO_4^{2-} + 5.86H_2O \quad (l0)$$

The transformation to the above semi-isocoulombic reaction is achieved by combination of Reaction (7) with the following reaction,

$$12.75 \times [H_2O(l) = H^+ + OH^-] \quad (11)$$

In the one-term isocoulombic approach for extrapolation, the equilibrium constants for Reaction (10) at the temperatures of interest are first calculated. Then, the solubility constants for saponite for Reaction (7) at the respective temperatures are retrieved by adding the equilibrium constants for Reaction (11) to those for Reaction (10). The equilibrium constants for Reaction (11) at the temperatures of interest are taken from EQ3/6 database, DATA0.YPF. The extrapolated solubility constants for saponite at temperatures close to 80 °C obtained in this way are listed in Table 4.

354 The saturation index, for the experimental solution of Debure et al. (2016) (see
355 their Table 3) at 90 °C is calculated (Table 5) with the solubility constant of saponite at
356 90 °C. Note that the chemical composition of my synthesized saponite is similar to that
357 reported by Debure et al. (2016) ("Phyllosilicate-Mg A"; see their Table 7). The
358 calculated saturation index is 0.54, indicating that the solution is saturated or slightly
359 supersaturated with saponite (Table 5). This is in good agreement with the experimental
360 observations that Mg-phyllosilicate did form in their experiment. As mentioned above,
361 the calculated saturation index is 0.54 (Table 5). Statistically speaking, the predictions
362 could encompass the exact saturation when the uncertainty associated with the solubility
363 constant of saponite at 90 °C (–67.6 ± 2.5, Table 4) is taken into consideration.
364 Thien et al. (2012) conducted glass corrosion experiments in synthetic ground
365 water (SGW) at 50 °C relevant to geological disposal of HLW. The SGW has the
366 chemical compositions that represent the ground water in equilibrium with the Callovo-
367 oxfordian argillite formation at Bure underground laboratory. The glasses they used were
368 AVM 6 and AVM 10 glasses; both of them containing magnesium as one of the
369 components. The AVM 6 glass was more enriched in SiO_2 than the AVM 10 glass. The
370 Mg-phyllosilicate (saponite) was precipitated in their experiments involving the AVM 6
371 glass.
372 Using the extrapolated solubility constant for saponite at 50 °C (Table 4), the
373 author calculated the saturation index for the experimental compositions of Thien et al.
374 (2012) involving the AVM 6 glass with the SGW at 50 °C. The calculated saturation
375 index is 0.71 (Table 6), indicating that saponite has a thermodynamic driving force for its

formation from the experimental solution. This is consistent with the experimental observations.

IMPLICATIONS AND CONCLUDING REMARKS

One important implication from this study is that when a nuclear waste glass is corroded in Mg-bearing solutions, Mg-saponite forms as a corrosion product, and the resulting solutions are close to be in equilibrium with Mg-saponite. Therefore, the solubility constants of Mg-saponite should be in the database as an essential part for prediction of the corrosion rates as a function of the solution chemistry in equilibrium with Mg-saponite.

Wilson *et al.* (2006) used the method proposed by Vieillard (2000) to estimate the Gibbs free energies of formation for smectites including Na-saponite with the stoichiometry of $Na_{0.70}(Mg_{6.00})[(Si_{7.30}Al_{0.70})O_{20}](OH)_4$. Notice that Wilson et al. (2000) used $O_{10}(OH)_2$ per formula unit for Na-saponite. To be consistent with $O_{20}(OH)_4$ per formula unit used in this study, their values are converted to those referring to $O_{10}(OH)_2$ per formula unit. They calculated the equilibrium constants for the dissolution of Na-saponite according to the following reaction,

$$Na_{0.70}(Mg_{6.00})[(Si_{7.30}Al_{0.70})O_{20}](OH)_4 + 14.8H^+ \rightleftharpoons 0.70Na^+ + 6\ Mg^{2+} + 0.70Al^{3+} + 7.30SiO_2(aq) + 9.4H_2O(l) \quad (12)$$

The $\log_{10} K^0$ for Reaction (12) at 80 °C estimated by Wilson et al. (2006) is 50.95 (uncertainty not provided, and the same is true with the following citations of the values from Wilson et al., 2006). The stoichiometry of their Na-saponite is very close to that of

This is the peer-reviewed, final accepted version for American Mineralogist, published by the Mineralogical Society of America.
The published version is subject to change. Cite as Authors (Year) Title. American Mineralogist, in press.
DOI: https://doi.org/10.2138/am-2021-7827. http://www.minsocam.org/

399 the saponite studied in this work, and therefore their estimated value can be compared
400 with the value determined in this study. In order to do a direct comparison with the
401 equilibrium constant at 80 °C determined in this study, Reaction (7) is transformed into
402 the following form,
403
404 $$Na_{0.95}Mg_{5.90}[(Si_{7.07}Al_{0.99})O_{20}](OH)_4 + 15.72H^+ \rightleftharpoons 0.95Na^+ + 5.90Mg^{2+}$$
405
406 $$+ 0.99Al^{3+} + 7.07SiO_2(aq) + 9.86H_2O(l) \quad (13)$$
407
408 by combining Reaction (7) with the following reactions,
409
410 $$H_2O(l) = H^+ + OH^- \quad (14)$$
411
412 $$SiO_2(aq) + 2H_2O(l) = 2H^+ + H_2SiO_4^{2-} \quad (15)$$
413
414 $$Al^{3+} + 4H_2O(l) = Al(OH)_4^- + 4H^+ \quad (16)$$
415
416 The equilibrium constants for Reactions (14) through (16) are from the EQ3/6 Data0.YPF
417 database, Xiong (2013), and Xiong (2014), respectively. Accordingly, the $\log_{10} K^0$ for
418 Reaction (13) at 80 °C is 70.30 ± 2.08. The $\log_{10} K^0$ estimated by Wilson et al. (2006)
419 differs from the experimentally determined value by ~20 orders of magnitude.
420 The estimated $\log_{10} K^0$ for Reaction (12) at 90 °C is 48.75 (Wilson et al. 2006), in
421 comparison with the extrapolated $\log_{10} K^0$ of 70.8 ± 2.5, based on the experimentally

This is the peer-reviewed, final accepted version for American Mineralogist, published by the Mineralogical Society of America.
The published version is subject to change. Cite as Authors (Year) Title. American Mineralogist, in press.
DOI: https://doi.org/10.2138/am-2021-7827. http://www.minsocam.org/

422 determined value. When the estimated $\log_{10} K^0$ is used to calculate the saturation index

423 ($\log \frac{Q}{K}$) of saponite for the solution chemistry from Debure et al. (2016) at 90 °C, the

424 saturation index is too high ($\log \frac{Q}{K} > 12$) to be consistent with the experimental

425 observations. Similarly, the estimated $\log_{10} K^0$ for Reaction (12) at 50 °C is 58.35

426 (Wilson et al. 2006), whereas the extrapolated $\log_{10} K^0$ is 70.4 ± 2.5. When the

427 estimated $\log_{10} K^0$ is applied to the solution chemistry at 50 °C from Thien et al. (2012),

428 the saturation index is too high ($\log \frac{Q}{K} > 12$) to be consistent with the experimental

429 observations. Consequently, in light of the experimental results presented in this work,

430 the estimation method needs to be revised to reconcile with the experimentally

431 determined values of this work and the experimental observations of Thien et al. (2012)

432 and Debure et al. (2016).

433 In addition, there is a solid phase of saponite-Na in the ThermoChimie database

434 (Giffaut et al., 2014; Blanc et al., 2015). The saponite-Na in the database has the

435 following stoichiometry on the basis of $O_{20}(OH)_4$ per formula unit:

436 $Na_{0.68}(Mg_{6.00})[(Si_{7.32}Al_{0.68})O_{20}](OH)_4$. The solubility constant ($\log_{10} K^0$) for dissolution

437 of the saponite-Na at 25 °C according to the following reaction

438 $$Na_{0.68}(Mg_{6.00})[(Si_{7.32}Al_{0.68})O_{20}](OH)_4 + 14.72H^+ \rightleftharpoons 0.68Na^+ + 6\ Mg^{2+}$$

439 $$+ 0.68Al^{3+} + 7.32H_4SiO_4(aq) + 9.4H_2O(l) \quad (12)$$

440 is 57.28 ± 7.30 based on the data set of 10a Version of September 26, 2018 (ANDRA,

441 2021). Notice that the error estimates are calculated based on the error percentage

442 relative to the basis of $O_{10}(OH)_2$ per formula unit in the original data set. The
443 extrapolated value at 25 °C for Reaction (13) is 72 ± 5, based on the value listed in
444 Table 4 in this study. When the quoted uncertainties and differences in stoichiometry are
445 taken into consideration, the estimated value from the ThermoChimie can be considered
446 to agree with the experimentally-based value at 25 °C. This is encouraging for the
447 estimation method, and it can be recalibrated with the experimental data at 25 °C
448 obtained in this study. In this way, the estimation method will be better to reconcile with
449 the experimental data and experimental observations, especially at elevated temperatures,
450 noted for the comparisons with the estimated values from Wilson *et al.* (2006), as the
451 ThermoChimie database and Wilson *et al.* (2006) use the same or very similar estimation
452 method.

453 In summary, the solubility constant of saponite with a stoichiometry of
454 $Na_{0.95}(Mg_{5.90}Al_{0.06})[(Si_{7.07}Al_{0.93})O_{20}](OH)_4$ at 80 °C has been determined in this work.
455 Then, the author extrapolated this value to other temperatures close to 80 °C (i.e., 50 °C,
456 60 °C, 70 °C, 90 °C, and 100 °C) by employing the one-term isocoulombic approach. The
457 author calculated the saturation indexes, $\log \frac{Q}{K}$, for the solution chemistry from the glass
458 corrosion experiments in the presence of a Mg-source at 50 °C and 90 °C from different
459 researchers. My calculated saturation indexes suggest that the solutions are
460 saturated/slightly-supersaturated with saponite, which are in close agreement with the
461 experimental observations at various temperatures. This suggests that the alteration
462 products containing Mg formed when glasses are corroded in a solution in the presence of
463 a Mg-source may control the chemical compositions, including hydrogen ion
464 concentrations, of the solutions in contact with the glasses. As the compositions of

465 natural saponite vary to some degree, the results are best applied to the situations where
466 the compositions of saponite are similar to those of synthetic saponite, such as the
467 saponite from Allt Ribhein, Skye.
468
469 **Acknowledgements**
470 Sandia National Laboratories is a multi-mission laboratory operated by National
471 Technology and Engineering Solutions of Sandia, LLC., a wholly owned subsidiary of
472 Honeywell International, Inc., for the U.S. Department of Energy's National Nuclear
473 Security Administration under contract DE-NA-0003525. This research is funded by Salt
474 R&D programs administered by the Office of Nuclear Energy (NE) of the U.S
475 Department of Energy. The views expressed in the article do not necessarily represent
476 the views of the U.S. Department of Energy or the United States Government. This paper
477 is published with the release number SAND2019-3740J. The author gratefully
478 acknowledges the laboratory assistance from Leslie Kirkes, Jandi Knox, Cassie Marrs,
479 Heather Burton, and Dick Grant. The author is grateful to the two journal reviewers for
480 their insightful and thorough reviews. Their reviews helped to improve the manuscript
481 significantly. The author thanks the Associate Editor (AE), Dr. Daniel Neuville, for his
482 editorial efforts, and the Editor, Dr. Hongwu Xu, for his editorial comments and his time.
483
484

REFERENCES

Abdelouas, A., Crovisier, J.-L., Lutze, W., Grambow, B., Dran, J.-C. & Müller, R. (1997) Surface layers on a borosilicate nuclear waste glass corroded in $MgCl_2$ solution. Journal of Nuclear Materials 240, 100–111.

ANDRA, (2021) www.thermochimie-tbd.com/pages/species-data.php. Accessed on April 19, 2021.

April, R.H. & Keller, D.M. (1992) Saponite and vermiculite in amygdales of the Granby basaltic tuff, Connecticut Valley. Clay and Clay Minerals 40, 22–31.

Aréna, H., Godon, N., Rébiscoul, D., Podor, R., Garcès, E., Cabie, M. & Metre, J.-P. (2016) Impact of Zn, Mg, Ni and Co elements on glass alteration: Additive effects. Journal of Nuclear Materials 470, 55–67.

Aréna, H., Godon, N., Rébiscoul, D., Frugier, P., Podor, R., Garces, E., Cabie, M. & Mestre, J.-P. (2017) Impact of iron and magnesium on glass alteration: Characterization of the secondary phases and determinations of the solubility constants. Applied Geochemistry 82, 119–133.

Bickmore, B.R., Nagy, K.L., Young, J.S., & Drexler, J.W. (2001) Nitrate-cancrinite precipitation on quartz sand in simulated Hanford tank solutions. Environmental Science and Technology 35, 4481–4486.

Bishop, J.L., Loizeau, D., McKeown, N.K., Saper, L., Dyar, M.D., Des Marais, D.J., Parente, M. & Murchie, S.L. (2013) What the phyllosilicates at Mawrth Vallis catell us about possible habitability on early Mars? Planetary and Space Science 86, 130–149.

Blanc, P., Vieillard, P., Gailhanou, H., Gaboreau, S., Marty, N., Claret, F., Made, B. & Giffaut, E., 2015. ThermoChimie database developments in the framework of cement/clay interactions. Applied Geochemistry 55, 95-107.

Bristow, T.F., Bish, D.L., Vaniman, D.T., Morris, R.V., Blake, D.F., Grotzing, J.P., Rampe, E.B., Crisp, J.A., Achilles, C.N., Ming, D.W. & Ehlmann, B.L. (2015) The origin and implications of clay minerals from Yellowknife Bay, Gale Crater, Mars. American Mineralogist 100, 824–836.

Cahoon, H. P. (1954) Saponite near Milford, Utah. American Mineralogist 19, 222–230.

Calvin, W.M., Lautze, N., Moore, J., Thomas, D., Haskins, E. & Rasmussen, B.P. (2020) Petrographic and spectral study of hydrothermal mineralization in drill core from Hawaii: A potential analog to alteration in the martian subsurface. American Mineralogist 105, 1297–1305.

Cuevas, J., De La Villa, V., Ramirez, S., Petit, S., Meunier, A. & Leguey, S. (2003) Chemistry of Mg smectites in lacustrine sediments from the Vicalvaro sepiolite, Madrid Neogene Basin (Spain). Clay and Clay Minerals 51, 457–472.

Curti, E., Crovisier, J. L., Morvan, G. & Karpoff, A. M. (2006) Long-term corrosion of two nuclear waste reference glasses (MW and SON68): A kinetic and mineral alteration study. Applied Geochemistry 21, 1152–1168.

Debure, M., De Windt, L., Frugier, P., Gin, S. & Vieillard, P. (2016) Mineralogy and thermodynamic properties of magnesium phyllosilicates formed during the alteration of a simplified nuclear glass. Journal of Nuclear Materials 475, 255–265.

Desprairies, A., Tremblay, P. & Laloy, C. (1989) Secondary mineral assemblage in a volcanic sequence drilled during ODP Leg 104 in the Norwegian Sea. Proceedings of the Ocean Drilling Program, Scientific Results, Vol. 104, 397–409.

Eberl, D.D., Whitney, G. & Khoury, H. (1978) Hydrothermal reactivity of smectite. American Mineralogist 63, 401–409.

Fleury, B., Godon, N., Ayral, A. & Gin, S. (2013) SON68 glass dissolution driven by magnesium silicate precipitation. Journal of Nuclear Materials 442, 17–28.

Frugier, P., Martin, C., Ribet, I., Advocat, T. & Gin, S. (2005) The effect of composition on the leaching of three nuclear waste glasses: R7T7, AVM, and VRZ. Journal of Nuclear Materials 346, 194–207.

Garvie, L.A.J. & Metcalfe, R. (1997) A vein occurrence of co-existing talc, saponite, and corrensite, Builth Wells, Wales. Clay Minerals 32, 223–240.

Gaucher, E. C., Tournassat, C., Pearson, F. J., Blanc, P., Crouzet, C., Lerouge, C. & Altmann, S. (2009) A robust model for pore-water chemistry of clayrock. Geochimica Cosmochimica Acta 73, 6470–6487.

Giffaut, E., Grivé, M., Blanc, P., Vieillard, P., Colàs, E., Gailhanou, H., Gaboreau, S., Marty, N., Made, B. & Duro, L., 2014. Andra thermodynamic database for performance assessment: ThermoChimie. *Applied Geochemistry*, *49*, pp.225-236.

Grambow, B. & Müller, R. (1989) Chemistry of glass corrosion in high saline brines. Materials Research Society Symposium Proceedings 176, 229–240.

Grambow, B. & Strachan, D. M. (1984) Leach testing of waste glasses under near-saturation conditions. Materials Research Society Symposium Proceedings, 623–634.

Gu, Y., Gammons, C.H. & Bloom, M.S. (1994) A one-term extrapolation method for estimating equilibrium constants of aqueous reactions at elevated temperatures. Geochimica et Cosmochimica Acta 58, 3545–3560.

Güven, N. (1990) Longevity of bentonite as buffer material in a nuclear-waste repository. Engineering Geology 28, 233–247.

Harrison, M.T. (2014) The effect of composition on short- and long-term durability of UK HLW glass. Procedia of Materials Science 7, 186–192.

He, H.-P., Li, T., Tao, Q., Chen, T.-H., Zhang, D., Zhu, J.-X., Yuan, P. & Zhu, R.-L. (2014) Aluminum ion occupancy in the structure of synthetic saponites: Effect on crystallinity. American Mineralogist 99, 109–116.

Hicks, L.J., Bridges, J.C. & Gurman, S.J. (2014) Ferric saponite and serpentine in the nakhlite martian meteorites. Geochimica et Cosmochimica Acta 74, 4605–4611

Hund, F. (1984) Nitrate-cancrinite, thiosulfate-cancrinite, sulfate-cancrinite, and sulfide-cancrinite. Z. Anorg. Allg. Chem, 509, 153–160.

565 Kadir, S. & Akbulut, A. (2003) The geology and origin of sepiolite, palygorskite and
566 saponite in Neogene lacustrine sediments of the Serinhisar-Acipayam Basin, Denizli,
567 southwestern Turkey. Clay and Clay Minerals 51, 279–292.

568 Kirkes, L. & Xiong, Y.-L. (2018) Experimental Determination of Brucite Solubility in
569 NaCl Solutions at Elevated Temperatures. In Xiong, Y.-L., ed., Solution Chemistry:
570 Advances in Research and Applications, pp. 48-68, Nova Science Publishers, New
571 York

572 Kohyama, N., Shimoda, S. & Sudo, T. (1973) Iron-rich saponite (ferrous and ferric
573 forms). Clay and Clay Minerals 21, 229–237.

574 Kong, X.Z., Tutolo, B.M. & Saar, M.O. (2013) DBCreate: A SUPCRT92-based program
575 for producing EQ3/6, TOUGHREACT, and GWB thermodynamic databases at user-
576 defined T and P. Computers & Geosciences 51, 415–417.

577 Lichtner, P.C. & Felmy, A.R. (2003) Estimation of Hanford SX tank waste compositions
578 from historically derived inventories. Computers & Geosciences 29, 371–383.

579 Liu, Q.Y., Xu, H.-W. & Navrosky, A. (2005) Nitrate cancrinite: Synthesis,
580 characterization, and determination of the enthalpy of formation. Microporous and
581 Mesoporous Materials 87, 146–152.

582 Luckscheiter, B. & Nesovic, M. (1998) Long term corrosion behaviour of the WAK-
583 HLW glass in salt solutions. Waste Management 17, 429–436.

584 Mackenzie, R.C. (1957) Saponite from Allt Ribhein, Fiskavaig Bay, Skye. Mineralogical
585 Magazine and Journal of the Mineralogical Society 31, 672–680.

586 Maeda, T., Ohmori, H., Mitsui, S. & Banba, T. (2011) Corrosion behavior of simulated
587 HLW glass in the presence of magnesium ion. International Journal of Corrosion
588 2011, Article ID 796457, 6 pages.

589 Mesmer, R.E. & Holmes, H.F. (1992) pH, definition and measurement at high
590 temperatures. Journal of Solution Chemistry 21, 725–744.

591 Nishri, A., Herbert, H. J., Jockwer, N. & Stichler, W. (1988) The geochemistry of brines
592 and minerals from the Asse Salt Mine, Germany. Applied Geochemistry 3, 317–332.

593 Post, J.L. (1984) Saponite from near Ballarat, California. Clay and Clay Minerals 32,
594 147–153.

595 Schuessler, W., Kienzler, B., Wilhelm, S., Neck, V. & Kim, J.I. (2001) Modeling of Near
596 Field Actinide Concentrations in Radioactive Waste Repositories in Salt Formations:
597 Effect of Buffer Materials. Materials Research Society Symposium Proceedings 663,
598 791–798.

599 Shao, H. & Pinnavaia, T.J. (2010) Synthesis and properties of nanoparticle forms
600 saponite clay, cancrinite zeolite and phase mixtures thereof. Microporous and
601 Mesoporous Materials 133, 10–17.

602 Sőhnel, O. & Novotný, P. (1985) Densities of aqueous solutions of inorganic substances.
603 Elsevier, New York, 335 p.

Strachan, D. M. (1983) Results from long-term use of the MCC-1 static leach test method. Nuclear and Chemical Waste Management 4, 177–188.

Strachan, D. M., Krupka, K. M. & Grambow, B. (1984) Solubility interpretations of leach tests on nuclear waste glass. Nuclear and Chemical Waste Management 5, 87–99.

Sueoka, Y., Yamashita, S., Kouduka, M. & Suzuki, Y. (2019). Deep microbial colonization in saponite-bearing fractures in aged basaltic crust: Implications for subsurface life on Mars. Frontiers in microbiology 10, Article 2793, 8 pages.

Tao, Q., Zeng, Q., Chen, M., He, H. & Komarneni, S., 2019. Formation of saponite by hydrothermal alteration of metal oxides: Implication for the rarity of hydrotalcite. *American Mineralogist: Journal of Earth and Planetary Materials*, *104*(8), pp.1156-1164.

Thien, B. M. J., Godon, N., Hulbert, F., Angeli, F., Gin, S. & Ayrol, A. (2010) Structural identification of a tri-octahedral smectite formed by the aqueous alteration of a nuclear glass. Applied Clay Science 49, 135–141.

Thien, B. M. J., Godon, N., Ballestero, A., Gin, S. & Ayrol, A. (2012) The dual effect of Mg on the long-term alteration rate of AVM nuclear waste glass. Journal of Nuclear Materials 427, 297–310.

U.S. National Academy of Sciences Committee on Waste Disposal. (1957) *The Disposal of Radioactive Waste on Land*. Publication 519. Washington, DC: National Academy of Sciences–National Research Council.

Utton, C.A., Hand, R.J., Hyatt, N.C., Swanton, S.W. and Williams, S.J. (2013) Formation of alteration products during dissolution of vitrified ILW in a high-pH calcium-rich solution. Journal of Nuclear Materials 442, 33–45.

Vieilard, P., 2000. A new method for the prediction of Gibbs free energies of formation of hydrated clay minerals based on the electronegativity scale. Clays Clay Minerals 48, 459–473.

Wilson, J., Savage, D., Cuadros, J., Shibata, M. & Ragnarsdottir, K.V. (2006) The effect of iron on montmorillonite stability. (I) Background and thermodynamic considerations. Geochimica et Cosmochimica Acta 70, 306–322.

Wolery, T.J. & Jarek, R.L. (2003) Software user's manual EQ3/6 (version 8.0). Sandia National Laboratories, Albuquerque/New Mexico.

Wolery, T.J., Xiong, Y.-L. & Long, J. (2010) Verification and Validation Plan/Validation Document for EQ3/6 Version 8.0a for Actinide Chemistry, Document Version 8.10. Carlsbad, NM: Sandia National laboratories. ERMS 550239.

Wood, S.A., Palmer, D.A., Wesolowski, D.J. & Bénézeth, P. (2002) The aqueous geochemistry of the rare earth elements and yttrium. Part XI. The solubility of $Nd(OH)_3$ and hydrolysis of Nd^{3+} from 30 to 290 ^{o}C at saturated water vapor pressure with in-situ pH_m measurement. In Hellmann, R. and Wood, S.A., ed., Water-Rock Interactions, Ore Deposits, and Environmental Geochemistry: A Tribute to David Crerar, Special Publication 7, The Geochemical Society, pp. 229–256.

644 Xiong, Y.-L. (2008) Thermodynamic properties of brucite determined by solubility
645 studies and their significance to nuclear waste isolation. Aquatic Geochemistry 14,
646 223–238.

647 Xiong, Y.-L. (2011) WIPP Verification and Validation Plan/Validation Document for
648 EQ3/6 Version 8.0a for Actinide Chemistry, Revision 1, Document Version 8.20.
649 Supersedes ERMS 550239. Carlsbad, NM. Sandia National Laboratories. ERMS
650 555358.

651 Xiong, Y.-L. (2013) A thermodynamic model for silica and aluminum in alkaline
652 solutions with high ionic strength at elevated temperatures up to 100 °C: Applications
653 to zeolites. American Mineralogist 98, 141–153.

654 Xiong, Y.-L. (2014) A Pitzer model for the Na-Al(OH)$_4$-Cl-OH system and solubility of
655 boehmite (AlOOH) to high ionic strength and to 250°C. Chemical Geology 373, 37–
656 49.

657 Xiong, Y.-L. (2015) Experimental determination of lead carbonate solubility at high ionic
658 strengths: a Pitzer model description. Monatshefte für Chemie-Chemical Monthly
659 146, 1433–1443.

660 Xiong, Y.-L. **(**2016**)** Solubility constants of hydroxyl sodalite at elevated temperatures
661 evaluated from hydrothermal experiments: Applications to nuclear waste isolation.
662 Applied Geochemistry 42, 1393–1403.

663 Xiong, Y.-L. & Lord, A.S. (2008) Experimental investigations of the reaction path in the
664 MgO–H_2O–CO_2 system in solutions with various ionic strengths, and their
665 applications to nuclear waste isolation. Applied Geochemistry 23, 1634–1659.

666 Xiong, Y.-L., Deng, H.-R., Nemer, M. & Johnsen, S. (2010) Experimental determination
667 of the solubility constant for magnesium chloride hydroxide hydrate
668 ($Mg_3Cl(OH)_5{\cdot}4H_2O$, phase 5) at room temperature, and its importance to nuclear
669 waste isolation in geological repositories in salt formations. Geochimica et
670 Cosmochimica Acta 74, 4605–4611.

671 Xiong, Y.-L. (2020) Experimental determination of the solubility constant of
672 kurnakovite. $MgB_3O_3(OH)_5{\bullet}5H_2O$. American Mineralogist 105, 977–983.

673 Xu, T., Pruess, K. & Brimhall, G. (1999) An improved equilibrium-kinetics speciation
674 algorithm for redox reactions in variably saturated subsurface flow systems.
675 Computers & Geosciences 25, 655–666.

676 Yang, T., Pusch, R., Knutsson, S. & Liu, X.-D. (2014) The assessment of clay buffers for
677 isolating highly radioactive waste. WIT Transactions on Ecology and The
678 Environment 180, 403–413.

679 Zhang, Z., Gan, X., Wang, L. & Xing, H. (2012) Alteration Development of the
680 Simulated HLW Glass at High Temperature in Beishan Underground Water.
681 International Journal of Corrosion 2012, Article ID 924963, 7 pages.

682

Figure Captions

Figure 1. XRD pattern of the solubility-controlling phases in the experiment performed in this work, compared with those of saponite 15A and NO_3-cancrinite.

Figure 2. SEM images and EDS analyses for the solid phases from the experiment performed in this study. A–C are SEM images with the respective EDS analyses: A. magnification at 6,500 times; B. magnification at 5,500 times; and C. magnification at 3,700 times.

Figure 3. A plot showing total molal concentrations of Al(III), Mg(II), Na(I), NO_3^-, and Si(IV) as a function of experimental time in an experiment approaching equilibrium from the direction of supersaturation at 80 ºC.

This is the peer-reviewed, final accepted version for American Mineralogist, published by the Mineralogical Society of America.
The published version is subject to change. Cite as Authors (Year) Title. American Mineralogist, in press.
DOI: https://doi.org/10.2138/am-2021-7827. http://www.minsocam.org/

Table 1. Chemical compositions of saponite synthesized in this work in comparison with those of natural saponite.

Oxide	Synthetic Saponite, This Work, wt%	Natural Saponite, Ballarat, California, wt% [A]	Natural Saponite, Milford, Utah, wt% [B]	Natural Saponite, Allt Ribhein, Fiskavaig Bay, Skye, wt% [C]
SiO_2	46.80	51.26	50.01	43.62
TiO_2	0.00	0.09	0.00	0.00
Al_2O_3	5.56	4.42	3.89	5.50
Fe_2O_3	0.00	1.14	0.21	0.66
FeO	0.00	---	0.00	---
MnO	0.00	0.03	0.00	0.06
MgO	26.22	23.54	25.61	24.32
CaO	0.00	1.25	1.31	2.85
Na_2O	3.27	1.14	0.00	0.08
K_2O	0.00	0.18	0.00	0.04
H_2O (LOI)	19.26 [D]	16.66	17.30	22.90

[A] Post (1984), $(Ca,Na,K)_{0.75}(Mg_{5.17}Al_{0.31}Fe^{III}_{0.13})[Si_{7.55}Al_{0.45}]O_{20}(OH)_4$. The stoichiometry is calculated in this work on the basis of $O_{20}(OH)_4$ per formula unit.

[B] Cahoon (1954), $(Ca,Na,K)_{0.42}(Mg_{5.72}Al_{0.19}Fe^{III}_{0.02})$ $[Si_{7.50}Al_{0.50}]O_{20}(OH)_4$. The stoichiometry is calculated in this work based on $O_{20}(OH)_4$ per formula unit..

[C] Mackenzie (1957), $(Na, K, Ca)_{1.02}(Mg_{5.84}, Mn_{0.01}, Al_{0.03}, Fe^{III}_{0.08})Si_{6.99}Al_{1.01}O_{20}(OH)_4$. The stoichiometry was calculated by Mackenzie (1957). I obtained almost the same formula based on the compositions provided.

[D] Based on TGA analysis up to 700 °C.

Table 2. Experimental data from the solubility experiment regarding the equilibrium between nitrate cancrinite and saponite produced in this study at 80.0 ± 0.5 °C.

Experimental Number	Experimental time, days	[A]pH_m	[B]m_{Na}	[B]$m_{\Sigma Mg(II)}$	[B]$m_{\Sigma Al(III)}$	[B]$m_{\Sigma Si(IV)}$	[C]$m_{NO_3^-}$	[D]m_{OH^-}
SAP-80-1	64	12.58	1.38	1.24E-05	2.94E-04	1.66E-02	6.72E-01	0.674
	85	12.56	1.42	1.11E-05	2.78E-04	1.99E-02	7.01E-01	0.674
	92	12.61	1.44	1.50E-05	1.94E-04	3.51E-02	6.91E-01	0.674

[A] Measured pH readings at 64, 85, 92 days were 12.43, 12.40, and 12.45, respectively, at the experimental temperature. The pH_m values are calculated by applying the correction factor at 80 °C from Kirkes and Xiong (2018) at the ionic strength of the experiment.
[B] Analyzed with ICP-AES
[C] Calculated based on charge balance
[D] Based on the initial NaOH concentration.

This is the peer-reviewed, final accepted version for American Mineralogist, published by the Mineralogical Society of America.
The published version is subject to change. Cite as Authors (Year) Title. American Mineralogist, in press.
DOI: https://doi.org/10.2138/am-2021-7827. http://www.minsocam.org/

Table 3. Equilibrium constants of saponite at 80 ± 0.5 °C determined in this work

Reactions	$\log_{10} Q^A$	$\log_{10} K^0$
$Na_{0.95}Mg_{5.90}[(Si_{7.07}Al_{0.99})O_{20}](OH)_4 + 2NO_3^- + 7.05Na^+ + 5.01Al(OH)_4^- \rightleftharpoons Na_8(Al_6Si_6O_{24})(NO_3)_2 \bullet 4H_2O + 5.90Mg^{2+} + 9.62OH^- + 1.07H_2SiO_4^{2-} + 2.14H_2O(l)$ (1)	–23.52 ± 1.96 (2σ)	–31.25 ± 1.96 (2σ)
$Na_8(Al_6Si_6O_{24})(NO_3)_2 \bullet 4H_2O + 12OH^- + 8H_2O(l) \rightleftharpoons 8Na^+ + 6Al(OH)_4^- + 6H_2SiO_4^{2-} + 2NO_3^-$ (4)		–37.99 ± 0.70 (2σ) [B]
$Na_{0.95}Mg_{5.90}[(Si_{7.07}Al_{0.99})O_{20}](OH)_4 + 2.38OH^- + 5.86H_2O(l) \rightleftharpoons 0.95Na^+ + 5.90Mg^{2+} + 0.99Al(OH)_4^- + 7.07H_2SiO_4^{2-}$ (7)		–69.24 ± 2.08 (2σ) [C]

[A] At ionic strength of 1.4 mol•kg^{-1}

[B] Based on a linear interpolation of the values at 89 °C (–36.20) from Bickmore et al. (2001) and at 75 °C (–39.03) from Lichtner and Felmy (2003).

[C] A combination of the reaction in Row 2 with that in Row 3 leads to the reaction in Row 4 and its corresponding equilibrium constant.

Table 4. Extrapolated equilibrium constants of saponite with the stoichiometry determined in this work at other temperatures close to 80°C

Reactions	T °C	$\log_{10} K^0$
$Na_{0.95}Mg_{5.90}[(Si_{7.07}Al_{0.99})O_{20}](OH)_4 + 2.38OH^- + 5.86H_2O(l) \rightleftharpoons 0.95Na^+ + 5.90Mg^{2+} + 0.99Al(OH)_4^- + 7.07H_2SiO_4^{2-}$	25	–80 ± 5 [C]
	50	–74.7 ± 2.5 [C]
	60	–72.8 ± 2.5 [C]
	70	–70.96 ± 2.5 [B]
	80	–69.24 ± 2.08 (2σ) [A]
	90	–67.6 ± 2.5 [C]
	100	–66.1 ± 2.5 [C]

[A] Determined in this study.

[B] One-term isocoulombic extrapolation based on the experimental value at 80 °C.

[C] Linear extrapolation in the space of log K vs. 1/T where T is in absolute temperature in K, based on the values at 70 °C and 80 °C.

Table 5. Chemical compositions of the solution in which the international simple glass was corroded at 90 °C

Concentration	ΣSi	ΣB	ΣNa	ΣAl	ΣCa	ΣMg
mmolar [A]	1.49E+00	1.1561E+02	6.298E+01	6.00E-02	5.00E-02	5.00E-02
mmolal [B]	1.55E+00	1.20E+02	6.55E+01	6.24E-02	5.20E-02	5.20E-02
Saturation state with respect to saponite, $Na_{0.95}Mg_{5.90}[(Si_{7.07}Al_{0.99})O_{20}](OH)_4$						
$\log \frac{Q}{K}$ [C]	0.5367					

[A] From Debure et al. (2016); concentration unit, 10^{-3} mol•dm^{-3}.

[B] This study, concentration unit, 10^{-3} mol•kg^{-1}. Converted from the results from Debure et al. (2016) by using a density of 0.15 mol•dm^{-3} NaCl at 90 °C to approximate the density of the experimental solution in Debure et al. (2016). The density of 0.15 mol•dm^{-3} NaCl at 90 °C is from Sőhnel and Novotný (1985).

[C] In $\log \frac{Q}{K}$, Q is ion activity product (IAP) with respect to saponite; K is the equilibrium constant defined by Reaction (7). In the calculation, pH was assumed to be constrained by the charge balance.

This is the peer-reviewed, final accepted version for American Mineralogist, published by the Mineralogical Society of America.
The published version is subject to change. Cite as Authors (Year) Title. American Mineralogist, in press.
DOI: https://doi.org/10.2138/am-2021-7827. http://www.minsocam.org/

Table 6. Chemical compositions of the solution in which the AVM 6 nuclear glass was corroded in synthetic groundwater (SGW) at 50 °C

Concentration	ΣSi	ΣB	ΣNa	ΣLi	ΣAl
mg/L [A]	19	786	2257	24	1.9
molar [B]	6.77E-04	7.27E-02	9.82E-02	3.46E-03	9.06E-05
molal [C]	6.86E-04	7.38E-02	9.96E-02	3.51E-03	9.19E-05
Concentration	ΣMg	ΣK	ΣCa	ΣCl	ΣSO_4
mg/L [A]	16	45	30	1491	1397
molar [B]	6.58E-04	1.15E-03	7.49E-04	4.21E-02	1.45E-02
molal [C]	6.68E-04	1.17E-03	7.59E-04	4.27E-02	1.48E-02
Saturation state with respect to saponite, $Na_{0.95}Mg_{5.90}[(Si_{7.07}Al_{0.99})O_{20}](OH)_4$					
$\log \frac{Q}{K}$ [D]	0.7075				

[A] From Thien et al. (2012), their experimental compositions involving the AVM 6 glass with the SGW at 219 days and 50 °C; concentration unit, 10^{-3} g•dm^{-3}.

[B] This study, concentration unit, mol• dm^{-3}; converted from the results of Thien et al. (2012). The calculated total ionic strength for the solution is 0.14 mol• dm^{-3}.

[C] This study, concentration unit, mol•kg^{-1}. Converted from the results on molar units by using a density of 0.14 mol•dm^{-3} NaCl at 50 °C to approximate the density of the SGW in which AVM 6 nuclear glass was corroded at 50 °C. The density of 0.14 mol•dm^{-3} NaCl at 50 °C is from Sőhnel and Novotný (1985).

[D] In $\log \frac{Q}{K}$, Q is ion activity product (IAP) with respect to saponite; K is the equilibrium constant defined by Reaction (7).

Appendix A. The elements, their lowest limits of detection, or LLD (wt.%), the crystal diffractometer used and counting times for EPMA analyses

Element	1-σ LLD (wt.%)	Crystal	Counting time (s)
Si	0.040	TAP [A]	20 sec Peak, 5 sec Background
Al	0.027	TAP	20 sec Peak, 5 sec Background
Mg	0.055	TAP	20 sec Peak, 5 sec Background
Na	0.050	TAP	20 sec Peak, 5 sec Background

[A] TAP, Thallium Acid Phthalate.

Appendix B. Comparison of major XRD peaks of saponite synthesized in this study with those of the saponite 15 Å standard (PDF-00-013-0086)*

Mg-saponite Standard, PDF-00-020-0964			Saponite, Synthesized in this study		
hkl	d-spacing, Å	Intensity	hkl	d-spacing, Å	Intensity**
(100)	4.57	50	(100)	4.572	166
(004)	3.67	60	(004)	3.666	214
(111)	2.58	20	(111)	2.577	242
(006)	2.42	20	(006)	2.421	217
(007)	2.09	30	(007)	2.089	82
(300)	1.53	90	(300)	1.534	111
(221)	1.32	40	(221)	1.322	76

*The major peaks with intensity ≥20 in the standard are compared with those in the synthetic saponite. The significant numbers presented for d-spacing of the synthesized saponite are one more than those presented in the PDF database for comparison. It is obvious that the synthesized saponite has the identical d-spacings when its significant numbers are rounded as the same significant numbers as the PDF database does.

** Experimental relative intensity

This is the peer-reviewed, final accepted version for American Mineralogist, published by the Mineralogical Society of America.
The published version is subject to change. Cite as Authors (Year) Title. American Mineralogist, in press.
DOI: https://doi.org/10.2138/am-2021-7827. http://www.minsocam.org/

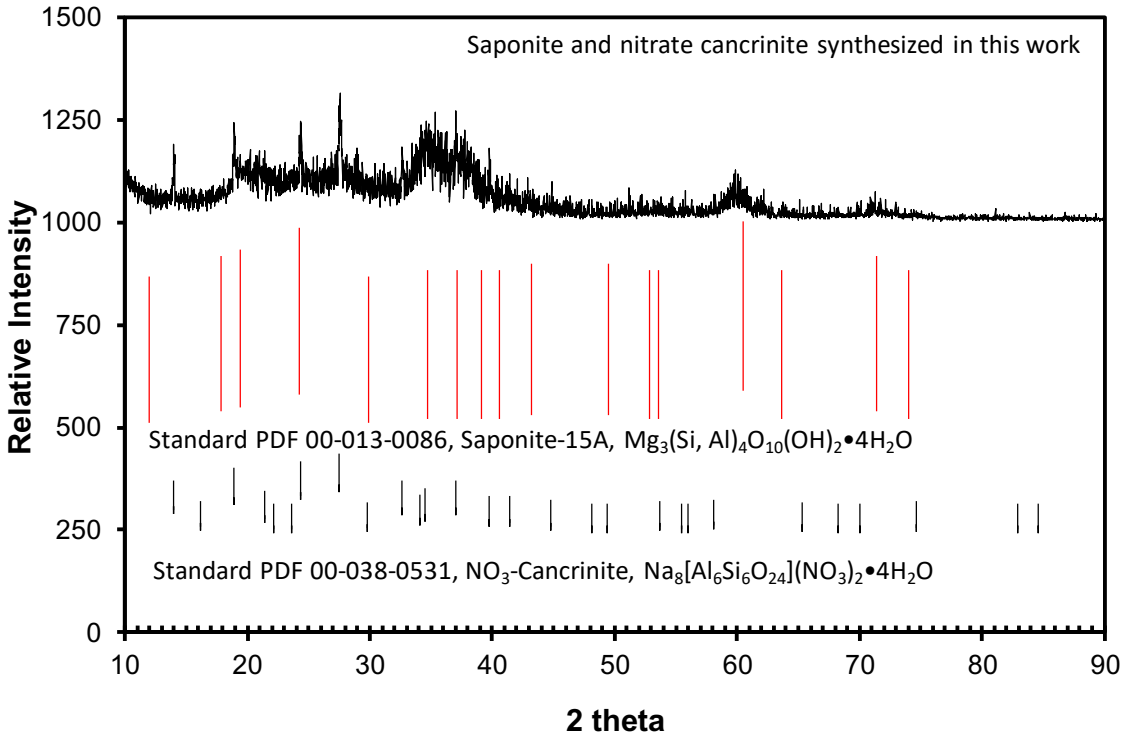

Figure 1.

822

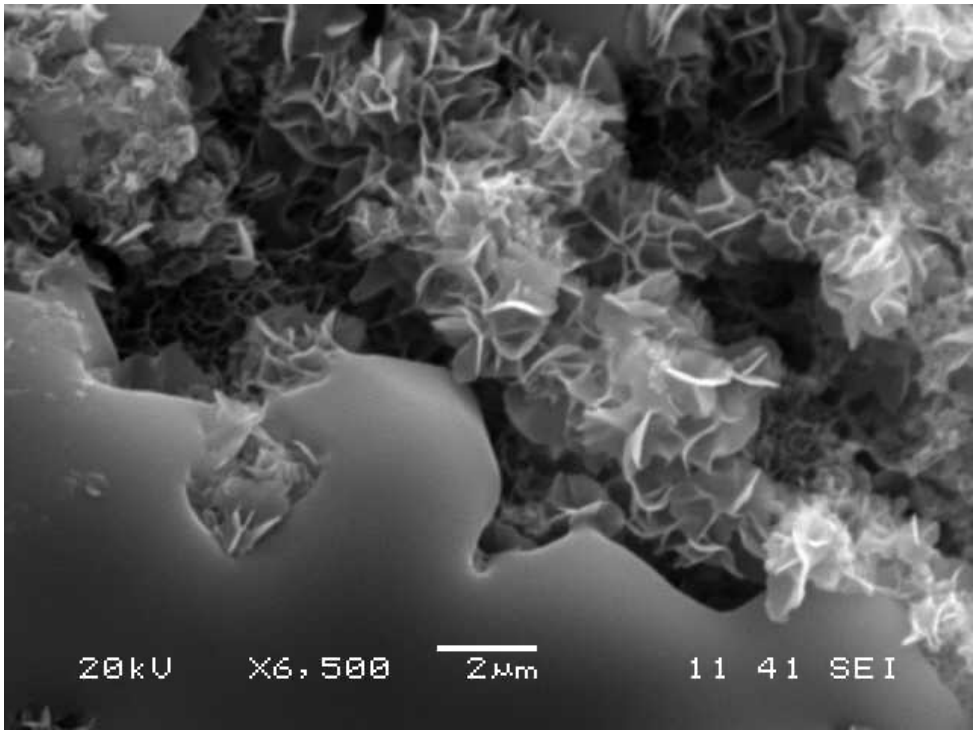

823
824

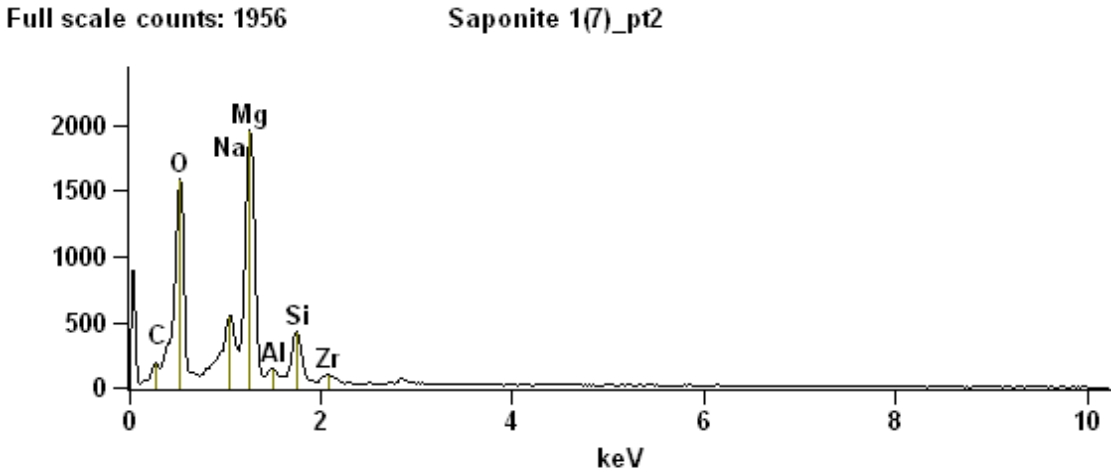

825
826
827
828 Figure 2A.
829

This is the peer-reviewed, final accepted version for American Mineralogist, published by the Mineralogical Society of America.
The published version is subject to change. Cite as Authors (Year) Title. American Mineralogist, in press.
DOI: https://doi.org/10.2138/am-2021-7827. http://www.minsocam.org/

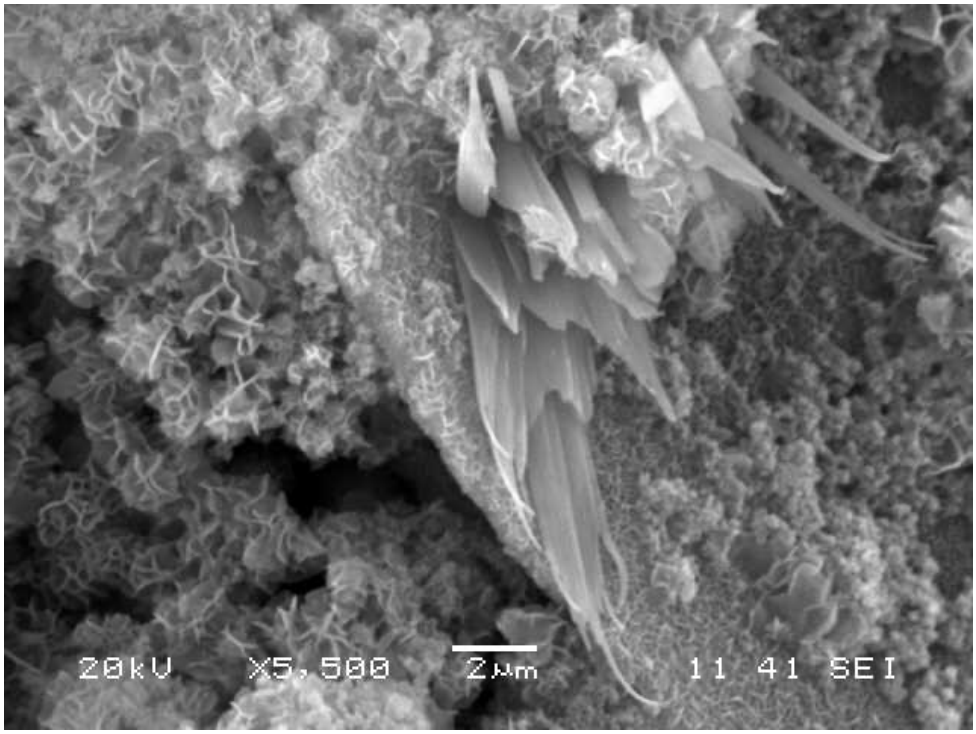

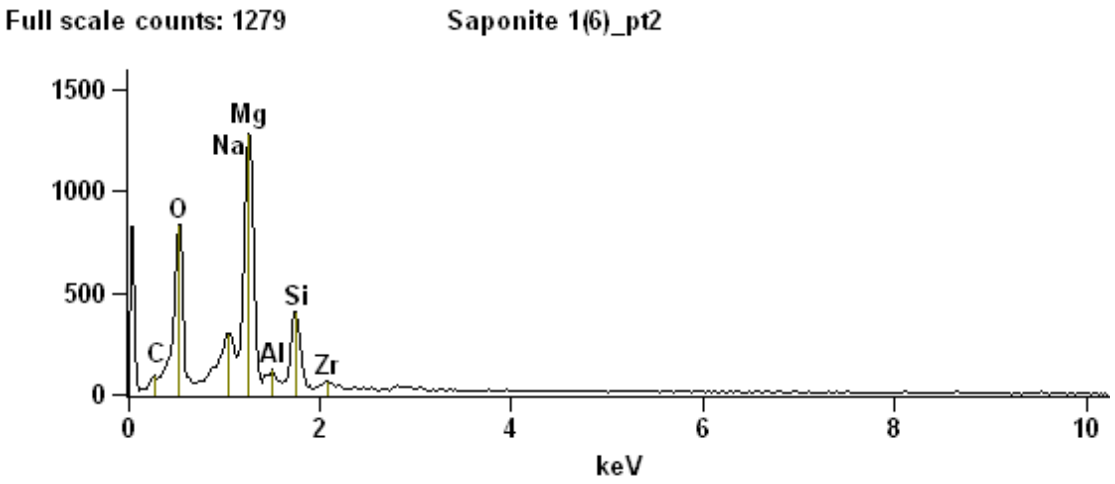

Figure 2B.

This is the peer-reviewed, final accepted version for American Mineralogist, published by the Mineralogical Society of America.
The published version is subject to change. Cite as Authors (Year) Title. American Mineralogist, in press.
DOI: https://doi.org/10.2138/am-2021-7827. http://www.minsocam.org/

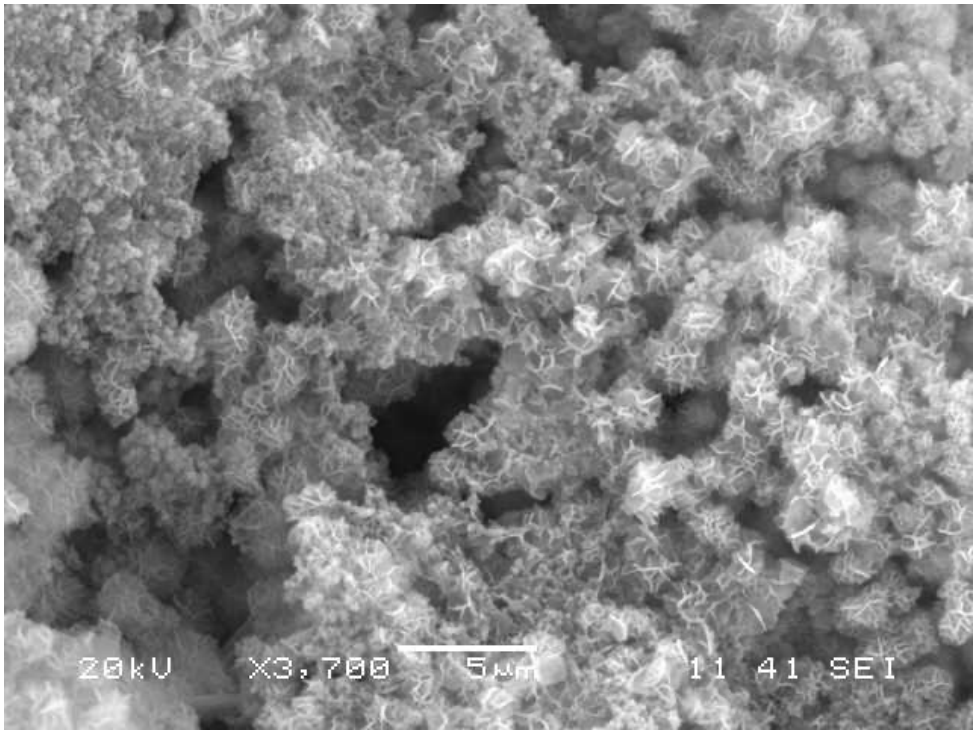

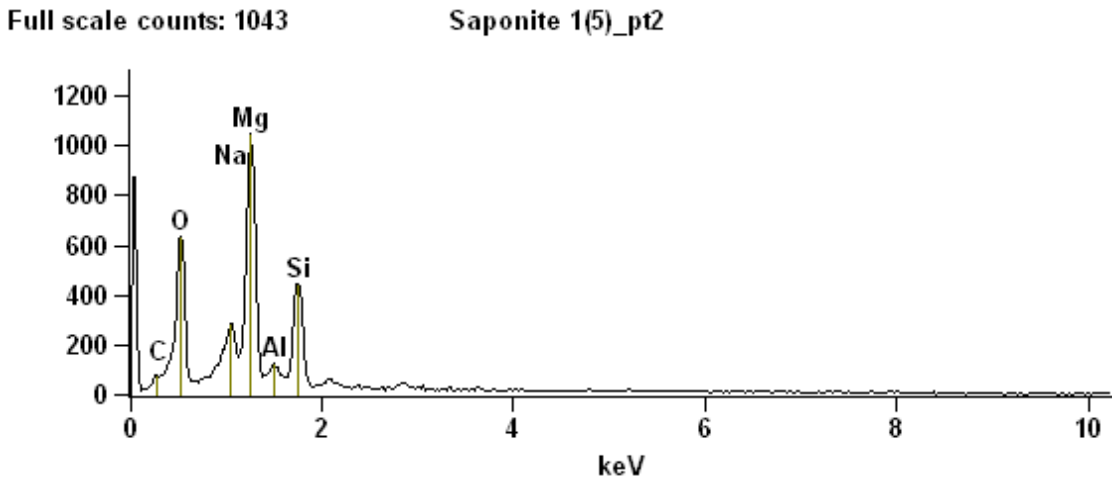

Figure 2C.

This is the peer-reviewed, final accepted version for American Mineralogist, published by the Mineralogical Society of America.
The published version is subject to change. Cite as Authors (Year) Title. American Mineralogist, in press.
DOI: https://doi.org/10.2138/am-2021-7827. http://www.minsocam.org/

858

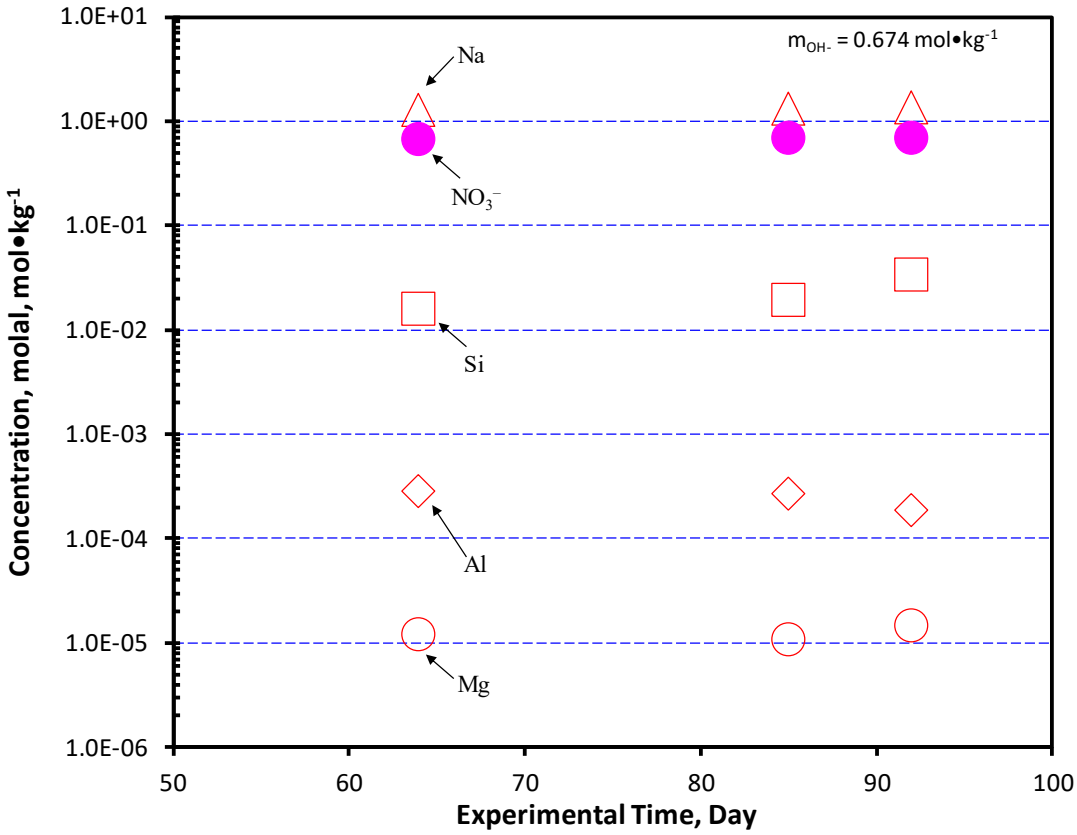

859
860
861 Figure 3.
862
863
864